

# STABILITY ANALYSIS METHOD OF SCATTERED-SHAPE UNSTABLE ROCK MASS

Yang An<sup>1\*</sup>, E-Chuan Yan<sup>2</sup>, Lin Li<sup>3</sup>, Xing-Ming Li<sup>4</sup>, and Shao-Ping Huang<sup>4</sup>

## ABSTRACT

Unstable rock is a common geological disaster in mountainous area in China. A rock of 0.01 m<sup>3</sup> rolling down in such crowded areas as scenic spots will cause serious accidents. The current norms don't include the stability analysis of small-diameter, and scattered-shape unstable rock. Based on traditional block theory, taking the cohesion and tensile strength of structural plane into account, the deformation and failure mechanical model of scattered-shape unstable rock mass under natural conditions was constructed. The calculation formula of net sliding force for block motion models including detachment from rock mass, sliding along one-sided and sliding along double-sided were derived according to unbalanced thrust method and vector analysis method. The stability coefficient of exemplified unstable rock mass was calculated by Visual Basic program language combined with Strength Reduction Method. Compared with 3DEC simulation results, which revealed the high similarity in both theoretical calculation and the numerical simulation in terms of the value of stability factor and expression of deformation and failure process, both of which were in coincident with reality. As an extension of and supplement to traditional block theory, the proposed stability calculating method for scattered-shape unstable rock mass has certain theoretical and engineering significance.

*Key words:* Scattered-shape unstable rock mass, block theory, stability analysis, strength reduction method, 3DEC.

## 1. INTRODUCTION

Unstable rock is a structural body composed of multiple groups of rock mass with structural planes on high steep slopes or cliffs, which is in unstable, under-stable or limit equilibrium state under the influence of inducing factors such as gravity and earthquake (Chen *et al.* 2003). Such a disaster is sudden and unpredictable. Despite the differences in massive loss of life and property caused by large collapse, the consequences of rockfall with small diameter are also tragic. On January 18, 2019, a falling rock on the road in Baihe Town, Yunnan hit a motorbike in motion, causing 3 deaths. The volume of this rockfall was only about 0.05 m<sup>3</sup>. On October 2, 2019, a rockfall incident in the Qixingzhai Scenic Area in Enshi Grand Canyon, which led to the death of three tourists and one injured. Through field investigation and analysis, we defined unstable rock mass cut by gently-dipping structural planes (such as bedding plane) and controlled by steep-dipping structural planes as scattered-shape unstable rock mass, which may break down layer by layer. Cut by dense structural planes, this kind of unstable rock mass is usually characterized by grid or chain morphology, scattered distribution pattern and small size rock blocks.

At present, the domestic and foreign literature on unstable rock mass mainly involves stability evaluation, deformation fail-

ure mechanism, prevention and control measures, *etc.* In terms of stability evaluation, Hu *et al.* (2011) established the evaluation criterion for unstable rock mass on the basis of stereographic projection method and divided the stability into 5 different zones. Chen *et al.* (2013) built the mutation instability model of unstable rock mass based on energy principle and mutation theory and proposed the calculation method for corresponding dynamic parameters. Cai *et al.* (2014) established the cantilever beam limit equilibrium model and verified its rationality with practical examples. Du *et al.* (2019) presented a method for reliability analysis of discontinuity-controlled rock mass on the basis of Monte Carlo method. Lin *et al.* (2013) analyzed the seepage coupling mechanism of Xiluodu arch dam foundation, where seepage pressure and water level fluctuation were considered. The relationship between permeability and stress-deformation of jointed rock mass was established. Liu *et al.* (2018) put forward multiscale hierarchical digital rock mass models which provided a unified and simple solution for determining the mechanical and hydraulic properties of rock mass in different scales. In terms of stability evaluation, Huang (2009) proposed the formation mechanism, geo-mechanical models and dynamic features of geological disasters triggered by Wenchuan 8.0 earthquake. Wang *et al.* (2014) analyzed deformation and failure pattern of layered anti-inclined rock slope under the action of natural and artificial factors. Four controlling factors for this kind slope evolution to collapse were summarized. Huang *et al.* (2016) judged the failure mode of a pillar-shaped rock mass in Three Gorges reservoir area as collapse by Hungr's quantitative discriminant (Hungr *et al.* 2014), which was consistent with the results of field investigation and monitoring. In terms of prevention and control measures, Liu *et al.* (1999) optimized a comprehensive treatment project for Lianziya unstable rock mass in Three Gorges of Yangtze River with the method of objective function. The continuous tracking optimization was also carried out. Huang *et al.* (2010) obtained the variation law of velocity and kinetic energy

Manuscript received June 6, 2021; revised August 12, 2021; accepted December 9, 2021.

<sup>1\*</sup> Ph.D. candidate (corresponding author), Faculty of Engineering, China University of Geosciences (Wuhan), Wuhan, China (e-mail: 657460276@qq.com).

<sup>2</sup> Professor, Faculty of Engineering, China University of Geosciences (Wuhan), Wuhan, China.

<sup>3</sup> Master, Faculty of Engineering, China University of Geosciences (Wuhan), Wuhan, China.

<sup>4</sup> Ph.D., Faculty of Engineering, China University of Geosciences (Wuhan), Wuhan, China.

during the collision between rolling rocks and trees based on the theory analysis of collision probability and field tests, whose conclusions serve as theoretical basis to the scheme design for unstable rock mass when trees were selected as passive protection. Wang *et al.* (2014) investigated the  $37.5 \times 10^4 \text{ m}^3$  giant unstable rock mass at the left dam abutment of Jiehu Hydropower Station on Yarlung Zangbo River in detail. Corresponding control measures were put forward on the basis of stability evaluation. Moon *et al.* (2014) presented a numerical approach to the design of rockfall catchfence based on rockfall stabilization works, which could be applied practically to optimize the design of rockfall barrier system under a given field condition. However, the literatures reported mainly concentrated on the unstable rock mass with certain scale. The research on scattered-shape unstable rock mass with small diameter was rarely mentioned.

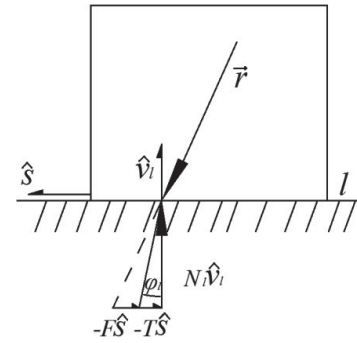
Block theory (Goodman and Shi 1985) has been widely used in the field of rock mass engineering since it was proposed. The discontinuity deformation analysis (DDA) method based on block theory plays an important role in rock mass stability evaluation (Shi and Goodman 1989). At present, the combination of 3D-DDA and unmanned aerial vehicle-laser scanner (UAV-LS) photogrammetry has become a new technology for stability analysis of discontinuity-controlled slopes (Liu *et al.* 2019). In traditional block theory, only the internal friction angle of structural plane was considered, whereas the cohesion and tensile strength of structural plane were ignored. The tensile strength of the structural planes in rock slope can reach tens of kPa. The failure mode is not only a single shear failure mode, but also a tension-shear composite failure mode (Dai *et al.* 2008; Lai *et al.* 2011). The impact of tensile strength on slope stability should be considered in engineering practice to avoid economic waste caused by over conservative design and potential danger caused by insufficient consideration of influencing factors (Lai *et al.* 2011). Once tensile strength of structural plane was considered, the transmission of sliding load between structural planes should also be considered simultaneously (Zhang and Jia 2019).

In consequence, based on traditional block theory, considering the cohesion and tensile strength of structural planes as well as transferring effect between blocks, the paper constructed the deformation and failure mechanical model of scattered-shape unstable rock. The calculation formula of net sliding force was deduced for 3 moving types after the instability of blocks, namely, detachment from rock mass, sliding along one-sided and sliding along double-sided. Visual Basic programming language combined with Strength Reduction Method (SRM) was used to calculate the stability coefficient of exemplified scattered-shape unstable rock mass. Comparing the theoretical calculation with the 3DEC numerical simulation analysis, there is a good similarity between their results. Moreover, both of them could reflect the actual failure phenomenon in practical engineering.

## 2. CALCULATION FORMULA OF NET SLIDING FORCE FOR ROCK BLOCK

### 2.1 Deformation and Failure Mechanical Model of Scattered-Shape Unstable Rock Mass

Traditional block theory mechanics analysis diagram is shown in Fig. 1.



**Fig. 1 Simplified diagram of traditional block theory mechanics analysis**

In this figure,  $\vec{F}$  is the resultant force of main active forces such as gravity, external water pressure and seismic force.  $\vec{F}$  is the virtual net sliding force in tangential direction of sliding structural plane.  $\hat{s}$  is the unit vector and parallels to the motion direction.  $N_l$  is the value of normal reaction force on sliding structure plane  $l$ .  $\hat{v}_l$  is unit normal vector of each structural plane of block pointing to the block itself.  $\hat{v}_l = I(a_l) \cdot \hat{n}_l$ , and  $I(a_l)$  is the corresponding value for structural plane  $l$  in symbol number of block theory.  $\phi_l$  is the internal friction angle of sliding structure plane  $l$ .  $\vec{N}$  is the resultant force of normal reaction force of sliding structure plane, which could be calculated by Eq. (1).  $\vec{T}$  is resultant force of anti-sliding force on sliding structure surface, it could be calculated by Eq. (2).

$$\vec{N} = \sum_l N_l \hat{v}_l \quad (1)$$

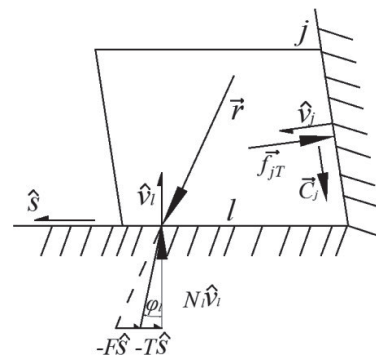
$$T = \sum_l N_l \tan \phi_l (-\hat{s}) \quad (2)$$

Based on this, the mechanical equilibrium equation of sliding block can be obtained:

$$\vec{F} + \sum_l N_l \hat{v}_l - (T + F)\hat{s} = 0$$

$$\text{or } F\hat{s} = \vec{F} + \sum_l N_l \hat{v}_l - T\hat{s} \quad (3)$$

Obviously, the traditional block theory failed to consider the tensile strength and cohesion of structural planes between blocks. With the consideration of these two factors, improved block mechanics analysis diagram for net sliding force calculation is shown in Fig. 2.



**Fig. 2 Simplified diagram of improved block theory mechanics analysis**

where:  $\vec{f}_{jT}$  is the tension provided by structural plane  $j$  when  $\hat{s} \cdot \hat{v}_j \geq 0$ . Because when it is an acute angle between unit normal vector  $\hat{v}_j$  and the motion direction, the structural plane  $j$  no longer provides support to the block. Which will trigger the tensile strength as one of the anti-sliding forces to prevent the block movement.  $\vec{C}_j$  is the cohesion provided by structural plane  $j$  when  $\hat{s} \cdot \hat{v}_j \geq 0$  and  $(\hat{s} \times \hat{v}_j) \times \hat{v}_j \cdot \hat{v}_l > 0$ . Among them,  $(\hat{s} \times \hat{v}_j) \times \hat{v}_j$  is the tangential component of  $\hat{s}$  on structural plane  $j$ . When the angle between  $(\hat{s} \times \hat{v}_j) \times \hat{v}_j$  and  $\hat{v}_l$  is an acute angle, it means that the direction of motion  $\hat{s}$  will produce a tangential component on structural plane  $j$  that is not geometrically constrained by the structural plane  $l$ . This will trigger the shear strength of structural plane  $j$ . Because  $\hat{s} \cdot \hat{v}_j \geq 0$ , structural plane  $j$  does not provide support to block, and the shear strength is provided by cohesion only.

In conclusion, when  $\hat{s} \cdot \hat{v}_j \geq 0$  and  $(\hat{s} \times \hat{v}_j) \times \hat{v}_j \cdot \hat{v}_l > 0$ , the sliding resistance for blocks is provided by tensile strength and cohesion of other structural planes except the sliding structural plane. Providing that once the structural plane is damaged, its tensile strength and shear strength will disappear at the same time. Therefore, sliding resistance depends on the short slab between the projection of tensile strength and the projection of cohesion on sliding surface in sliding direction. After the active resultant force in Fig. 2 is merged with all forces on sliding surface  $l$ , there is a remaining active resultant force  $\vec{r}'$ , as is illustrated in Fig. 3. If the angle between  $\hat{s}$  and  $\hat{v}_j$  is acute, the projection on normal direction of structural surface of  $\vec{r}'$  pointing to block itself is  $|\vec{r}'| \cos \theta$  and the projection on tangential direction is  $|\vec{r}'| \sin \theta$ . In the process of gradual increase of  $\vec{r}'$ , if  $|\vec{r}'|$  exceeds  $\vec{f}'$  first, structural plane will undergo tensile failure, and the shear strength will be  $|\vec{f}_{jT}| \tan \theta$ . If  $|\vec{r}'|$  exceeds  $|\vec{C}_j|$  first, structural plane will undergo shear failure, and the tensile strength will be  $|\vec{C}_j| \cot \theta$ . In other words, how much the resistance provided by non-sliding structural plane entirely depends on the smaller value between  $|\vec{f}_{jT}| / \cos \theta$  and  $|\vec{C}_j| \sin \theta \cdot \tan \theta = |\hat{s} \times \hat{v}_j| / |\hat{s} \cdot \hat{v}_j|$ , the formula could be derived:

$$\vec{F}_{jR} = \vec{f}_{jT} + \frac{|\vec{f}_{jT}| |\hat{s} \times \hat{v}_j|}{s \cdot v_j} \frac{(\hat{s} \times \hat{v}_j) \times \hat{v}_j}{|(\hat{s} \times \hat{v}_j) \times \hat{v}_j|} \quad \text{Tensile failure}$$

$$\vec{F}_{jR} = \{ \vec{C}_j + \frac{|\vec{C}_j| |\hat{s} \times \hat{v}_j|}{|\hat{s} \cdot \hat{v}_j|} \cdot (-\hat{v}_j) \} \quad \text{Shear failure} \quad (4)$$

$$\vec{C}_j = \frac{c_j a_j \cdot \hat{v} \times (\hat{s} \times \hat{v}_j)}{|\hat{s} \times \hat{v}_j|} \quad (5)$$

$$\vec{f}_{jT} = \sigma_{jT} \cdot a_j \cdot (-\hat{v}_j) \quad (6)$$

where:  $\vec{F}_{jR}$  is the resistance provided by non-sliding structural plane  $j$ ,  $C_j$  is the tensile strength of structural plane  $j$ , and  $a_j$  is the penetrating failure area of structural plane  $j$ . The direction of  $\vec{F}_{jR}$  is opposite to the motion direction,  $\vec{F}_{jR} = |\vec{F}_{jR}| \cdot (-\hat{s})$ .

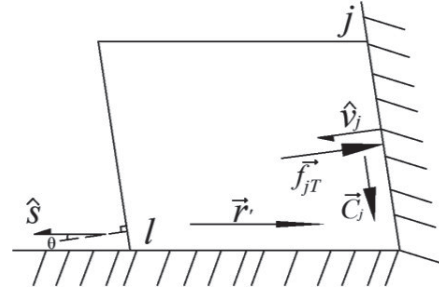


Fig. 3 Simplified diagram of non-sliding structural plane for failure mechanics analysis

When  $\hat{s} \cdot \hat{v}_j \geq 0$  and  $(\hat{s} \times \hat{v}_j) \times \hat{v}_j \cdot \hat{v}_l \leq 0$ , tangential component of  $\hat{s}$  on structural plane  $j$  will not be geometrically constrained by the structural plane  $l$ . It will not trigger the shear strength of structural plane  $j$ . In this context, the resistance provided by structural plane is the projection of tension on the motion direction:

$$\vec{F}_{jR} = \vec{f}_{jT} \cdot \hat{s} \cdot \hat{s} \quad (7)$$

Based on the above analysis, traditional block theory has been improved. Eq. (2) could be changed to:

$$\vec{T} = \sum_l N_l \tan \varphi_l (-\hat{s}) + \sum_l \vec{C}_l + \sum_j \vec{F}_{jR} \quad (8)$$

## 2.2 Detachment from Rock Mass

When the angle between the direction of active resultant force and the unit normal vector pointing to block inside of each structural plane is an acute angle, every structure plane has no supporting effect on block, thus the block separates from rock mass. That is:

$$\begin{cases} \hat{s} = \hat{r} \\ \hat{s} \cdot \hat{v}_l > 0 \end{cases} \quad (9)$$

The blocks are numbered in turn, and the calculation diagram is shown in Fig. 4. Block 1 is taken for analysis, and Eq. (3) can be written as:

$$F^{(1)} \hat{s} = \vec{r} + \sum_l \vec{F}_{lR}^{(1)} - \sum_j \vec{F}_{jR}^{(1)} \quad (10)$$

where  $l$  is structural plane that meets the condition of  $(\hat{s} \times \hat{v}_l) \times \hat{v}_l \cdot \hat{s} > 0$ . That is, it could trigger both shear and tensile strength meanwhile, such as the two sides in Fig. 3.  $j$  is the structural plane that meets the condition of  $(\hat{s} \times \hat{v}_j) \times \hat{v}_j \cdot \hat{s} \leq 0$ , which only triggers tensile strength, such as the bedding plane in Fig. 4. Superscript "(1)" refers to the resistance provided by structural plane in contact with Block 1. With the tensile force transmission effect of structural plane, when block number  $n \geq 2$ , the net sliding force of block is:

$$F^{(n)} \hat{s} = \vec{r} + \sum_j \vec{F}_j^{(n-1)} - \sum_l \vec{F}_l^{(n)} - \sum_j \vec{F}_j^{(n)} \quad (11)$$

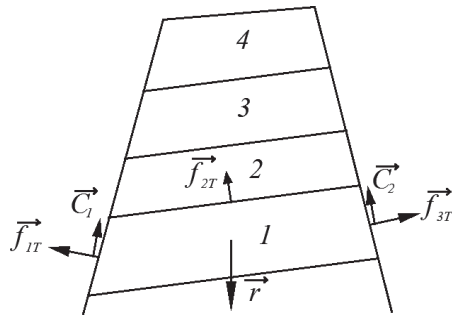


Fig. 4 Simplified diagram of detachment form rock mass

### 2.3 Along One-Sided Sliding

If a block slides along a single structural plane  $l$ , the moving direction of block should be consistent with the projection direction of active force on this plane, namely:

$$\hat{s} = \hat{s}_l = \frac{(\hat{v}_l \times \hat{r}) \times \hat{v}_l}{|\hat{v}_l \times \hat{r}|} \quad (12)$$

At the same time, it should be ensured that block will not be separated from structural plane  $l$  under the action of active resultant force  $\vec{r}$ . In addition, block should separate from the rest structural plane  $j$ , that is:

$$\begin{cases} \hat{r} \cdot \hat{v}_l \leq 0 \\ \hat{s} \cdot \hat{v}_j > 0 \end{cases} \quad (13)$$

The calculation diagram is shown in Fig. 5. Taking the lowest block for analysis, Eq. (3) can be written as following form:

$$F\hat{s} + \vec{r} + N\hat{v} + \vec{T} = 0 \quad (14)$$

By substituting Eq. (8) with Eq. (14), the formula can be derived as following:

$$F\hat{s} = -\vec{r} - N_l\hat{v}_l + N_l \tan \varphi_l \hat{s} - \vec{C}_l - \sum_j \vec{F}_{jR} \quad (15)$$

Because of  $\hat{s} \cdot \hat{v}_l = 0$ ,  $\vec{C}_l = |\vec{C}_l| \cdot (-\hat{s})$ ,  $\sum_j \vec{F}_{jR} = |\sum_j \vec{F}_{jR}| \cdot (-\hat{s})$ , it yields:

$$F = -|\vec{r}| \cdot \hat{r} \cdot \hat{s} + N_l \tan \varphi_l + |\vec{C}_l| + |\sum_j \vec{F}_{jR}| \quad (16)$$

Perform the right cross product  $\hat{s}$  on both sides of Eq. (8):

$$N_l(\hat{v}_l \times \hat{s}) = -|\vec{r}|(\hat{r} \times \hat{s}) \quad (17)$$

Substitute Eq. (12) with Eq. (17):

$$N_l \frac{\hat{v}_l \times (\hat{v}_l \times \hat{r}) \times \hat{v}_l}{|\hat{v}_l \times \hat{r}|} = -|\vec{r}| \frac{\hat{r} \times (\hat{v}_l \times \hat{r}) \times \hat{v}_l}{|\hat{v}_l \times \hat{r}|} \quad (18)$$

According to the Lagrangian cross product formula, the numerator of left term in Eq. (18) can be simplified into  $\hat{v}_l \times \hat{r}$ , the numerator of right term can be simplified into  $(\hat{v}_l \times \hat{r}) \cdot (\hat{r} \cdot \hat{v}_l)$ . Equation (18) could be changed into:

$$N_l = -|\vec{r}|(\hat{r} \cdot \hat{v}_l) \quad (19)$$

Thereinto,  $\hat{r} \cdot \hat{v}_l < 0$ , Eq. (19) can be written as:

$$N_l = |\vec{r}| |\hat{r} \cdot \hat{v}_l| \quad (20)$$

Substituting Eq. (20) with Eq. (16), net sliding force of block at the bottom can be achieved:

$$F = |\vec{r}| (|\hat{r} \cdot \hat{v}_l| \tan \varphi_l - \hat{r} \cdot \hat{s}) + |\vec{C}_l| + |\sum_j \vec{F}_{jR}| \quad (21)$$

Number scattered-shape unstable rock blocks from bottom to top in the moving direction. When block number  $n \geq 2$ , if the net sliding force of Block  $n - 1$  meets the condition of:

$$0 < F^{n-1} < |\sum_j \vec{F}_{jR}^{(n-1)}| \quad (22)$$

The shear strength of sliding plane is not enough to keep block stable, which will trigger the tensile strength of top structural plane. Therefore, the projection  $(|\sum_j \vec{F}_{jR}^{(n-1)}| - F^{n-1})$  of tension generated by Block  $n - 1$  on sliding plane should be counted in the calculation of net sliding force of the Block  $n$ . The following result could be obtained:

$$F^{(n)} = |\vec{r}^{(n)}| (|\hat{r} \cdot \hat{v}_l| \tan \varphi_l - \hat{r} \cdot \hat{s}) + |\vec{C}_l^{(n)}| + |\sum_j \vec{F}_{jR}^{(n-1)}| \quad (23)$$

If the net sliding force of Block  $n - 1$  meets the condition of Eq. (24), shear strength of sliding plane is sufficient to maintain the stability of block without tension to non-sliding structural plane on the top. Then, after deducting the resistance of top non-sliding structural plane, the remaining sliding force of Block  $n - 1$  can be superposed to Block  $n$ . The expression of  $F^{(n)}$  is the same as in the above case, as is shown in Eq. (23).

$$0 < |\sum_j \vec{F}_{jR}^{(n-1)}| < F^{n-1} \quad (24)$$

When  $F^{n-1} \leq 0$ , it means that Block  $n - 1$  is have been unstable or in extreme equilibrium state. The tensile force generated by top non-sliding structural plane is totally transmitted to lower part. Then  $|\sum_j \vec{F}_{jR}^{(n-1)}|$  should be deducted when calculating the net sliding force of Block  $n$ . That is to say:

$$F^{(n)} = |\vec{r}^{(n)}| (|\hat{r} \cdot \hat{v}_l| \tan \varphi_l - \hat{r} \cdot \hat{s}) + |\vec{C}_l^{(n)}| + |\sum_j \vec{F}_{jR}^{(n)}| - |\sum_j \vec{F}_{jR}^{(n-1)}|$$

To sum up, the calculation method of net sliding force when block number  $n \geq 2$  is:

$$\begin{cases} |\vec{r}^{(n)}| (|\hat{r} \cdot \hat{v}_l| \tan \varphi_l - \hat{r} \cdot \hat{s}) + |\vec{C}_l^{(n)}| + |\sum_j \vec{F}_{jR}^{(n)}| + F^{(n-1)} - |\sum_j \vec{F}_{jR}^{(n-1)}|, & F^{(n-1)} > 0 \\ |\vec{r}^{(n)}| (|\hat{r} \cdot \hat{v}_l| \tan \varphi_l - \hat{r} \cdot \hat{s}) + |\vec{C}_l^{(n)}| + |\sum_j \vec{F}_{jR}^{(n)}| - |\sum_j \vec{F}_{jR}^{(n-1)}|, & F^{(n-1)} \leq 0 \end{cases} \quad (26)$$

According to Eq. (26), the net sliding force of each block could be calculated step by step from the bottom of scattered-shape unstable rock mass. Since net sliding force is transferred from bottom to top, when Block  $k$  appears and the situation of  $F^{(k)} < 0$ , it indicates that Block  $1 \sim k$  have been unstable.

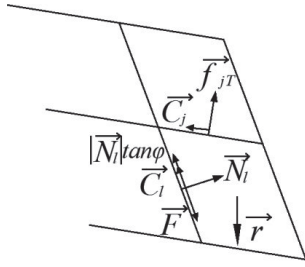


Fig. 5 Simplified diagram of along one-sided sliding

### 2.4 Along Double-Sided Sliding

If block slides along both sides of structural plane  $i$  and  $l$ , the block actually slides along intersected line. Then its motion direction is:

$$\hat{s} = s_{il} = \frac{I^{il}}{|\vec{I}_{il}|} \cdot \text{sign}(\vec{I}_{il} \cdot \vec{r}) \quad (27)$$

In this case, block must be in contact with the structural planes  $i$  and  $l$ , while separated from structural plane  $j$ :

$$\begin{cases} \hat{s}_i \cdot \hat{v}_l \leq 0 \\ \hat{s}_l \cdot \hat{v}_i \leq 0 \\ \hat{s} \cdot \hat{v}_j > 0 \end{cases} \quad (28)$$

where: red lines and green lines represent surface plane  $i$  and  $l$ , respectively while blue lines represent non-sliding surface plane  $j$ . Take Block 11 in Fig. 6 for analysis, as is shown in Fig. 7. Equation (3) can be written in the following form:

$$F\hat{s} = -\vec{r} - N_l \hat{v}_l - N_i \hat{v}_i + N_l \tan \phi_i \hat{s} + N_i \tan \phi_i \hat{s} - \vec{C}_l - 2\vec{C}_i - \vec{F}_{jR} \quad (29)$$

Although both sides of block have cohesion, the left side does not provide support because the angle between unit normal vector pointing to block itself and active resultant force is acute. For blocks sliding along both sides,  $\hat{s} \cdot \hat{v}_l = 0$ ,  $\hat{s} \cdot \hat{v}_i = 0$ ,  $\vec{C}_l = |\vec{C}_l| \cdot (-\hat{s})$ ,  $\vec{C}_i = |\vec{C}_i| \cdot (-\hat{s})$  and  $\vec{F}_{jR} = |\vec{F}_{jR}| \cdot (-\hat{s})$ .

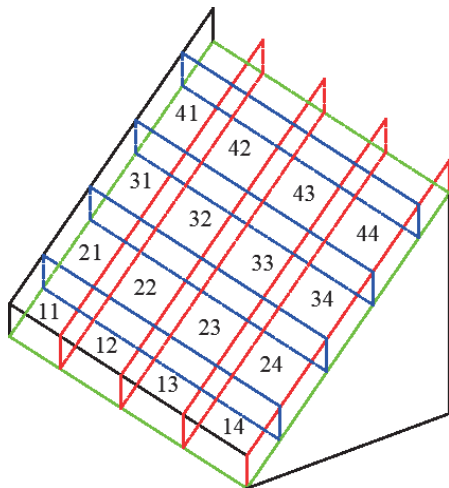


Fig. 6 Simplified diagram of along double-sided sliding

$$F = -|\vec{r}| \cdot \hat{r} \cdot \hat{s} + N_l \tan \phi_l + N_i \tan \phi_i + |\vec{C}_l| + 2|\vec{C}_i| + \vec{F}_{jR} \quad (30)$$

Take cross product  $\hat{v}_l$  on Eq. (30) first, then apply dot product of  $\hat{v}_l \times \hat{v}_i$ , the following result could be obtain:

$$F(\hat{s} \times \hat{v}_l) \cdot (\hat{v}_l \times \hat{v}_i) = -|\vec{r}| \cdot (\hat{r} \times \hat{v}_l) \cdot (\hat{v}_l \times \hat{v}_i) + N_l (\hat{v}_l \times \hat{v}_i) \cdot (\hat{v}_l \times \hat{v}_i) + (N_l \tan \phi_l + N_i \tan \phi_i - |\vec{C}_l| - 2|\vec{C}_i| + |\vec{F}_{jR}| \cdot (\hat{s} \times \hat{v}_l)) \cdot (\hat{v}_l \times \hat{v}_i) \quad (31)$$

As  $\hat{s}$  is parallel to  $(\hat{v}_l \times \hat{v}_i)$ ,  $(\hat{s} \times \hat{v}_l) \cdot (\hat{v}_l \times \hat{v}_i) = (\hat{v}_l \times \hat{v}_i) \times \hat{s} \cdot \hat{v}_l = 0$ . Equation (31) could be simplified as:

$$|\vec{r}| \cdot (\hat{r} \times \hat{v}_l) \cdot (\hat{v}_l \times \hat{v}_i) = N_l (\hat{v}_l \times \hat{v}_i) \cdot (\hat{v}_l \times \hat{v}_i) \quad (32)$$

$$N_l = \frac{(\vec{r} \times \hat{v}_l) \cdot (\hat{v}_l \times \hat{v}_i)}{|\hat{v}_l \times \hat{v}_i|^2} \quad (33)$$

In the same way:

$$N_i = \frac{(\vec{r} \times \hat{v}_i) \cdot (\hat{v}_l \times \hat{v}_i)}{|\hat{v}_l \times \hat{v}_i|^2} \quad (34)$$

Transform Eqs. (33) and (34) into Eq. (30), the net sliding force of Block 11 could be calculated by Eq. (35)

$$F = -|\vec{r}| \cdot \hat{r} \cdot \hat{s} + \frac{(\vec{r} \times \hat{v}_l) \cdot (\hat{v}_l \times \hat{v}_i)}{|\hat{v}_l \times \hat{v}_i|^2} \tan \phi_l + \frac{(\vec{r} \times \hat{v}_i) \cdot (\hat{v}_l \times \hat{v}_i)}{|\hat{v}_l \times \hat{v}_i|^2} \tan \phi_i + |\vec{C}_l| + 2|\vec{C}_i| + \vec{F}_{jR} \quad (35)$$

Next, consider transmission effect of net sliding force in horizontal direction. Taking Block 1b ( $b \geq 2$ ) as an example, and its force diagram is shown in Fig. 8. Force  $\vec{N}_i + |\vec{N}_i| \tan \phi + \vec{C}_i$  on the left side is the reaction force of supporting force and frictional resistance on the right side of Block 1( $b-1$ ). In order to maintain the balance of block in normal direction of structural plane  $i$ ,  $N_i + |N_i| \tan \phi$  is added to the supporting force generated by its own weight on the right side of Block 1b. The direction is opposite to that of the reaction force on the left side and their values are equal. They can be cancelled out. Hence, Eq. (3) should be written in the following form for Block 1b.

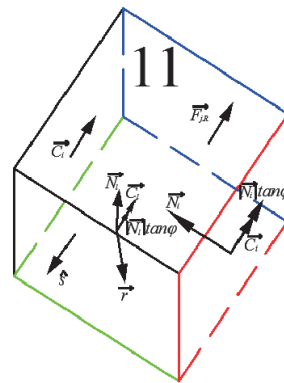


Fig. 7 Simplified diagram of Block 11 for analysis

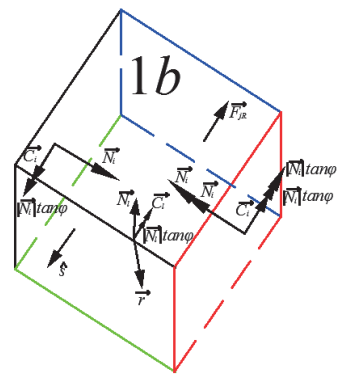


Fig. 8 Simplified diagram of Block 1b for analysis

$$\begin{aligned}
 F^{(1b)} \hat{c} = & -\bar{r}^{(1b)} - N_i^{(1b)} \hat{v}_i - N_l^{(1b)} \hat{v}_l + N_l^{(1b)} \tan \varphi_l \hat{s} \\
 & + N_i^{(1b)} \tan \varphi \hat{s}_i - \bar{C}_i^{(1b)} - (C_i^{(1b)} - \bar{C}_i^{[1(b-1)]} - F_{jR}^{(1b)})
 \end{aligned} \quad (36)$$

With similar to previous derivation process, it is easy to get the formula for calculating the net sliding force of Block 1b.

$$\begin{aligned}
 F^{(1b)} = & -|\bar{r}^{(1b)}| \cdot \hat{r} \cdot \hat{s} + |\bar{C}_i^{(1b)}| + |\bar{F}_{jR}^{(1b)}| - |\bar{C}_i^{(1b)} - \bar{C}_i^{[1(b-1)]}| \\
 & + \frac{(\bar{r}^{(1b)} \times \hat{v}_i) \cdot (\hat{v}_i \times \hat{v}_l)}{|\hat{v}_i \times \hat{v}_l|^2} \tan \varphi_l + \frac{(\bar{r}^{(1b)} \times \hat{v}_l) \cdot (\hat{v}_i \times \hat{v}_l)}{|\hat{v}_i \times \hat{v}_l|^2} \tan \varphi_i
 \end{aligned} \quad (37)$$

Through iterative calculation, net sliding force of Block 1b ( $b \geq 2$ ) in the bottom row can be obtained. Now, consider transmission effect of net sliding force in vertical direction (Block 21, Block 31, *et al*). Taking Block a1 ( $a \geq 2$ ) as an example, analysis idea is consistent with above-mentioned upward transmitting idea of net sliding force in Section 3.2. Therefore, formula for calculating the net sliding force of Block a1 can be obtained.

$$\begin{aligned}
 F^{(a1)} = & -|\bar{r}^{(a1)}| \cdot \hat{r} \cdot \hat{s} + \frac{(\bar{r}^{(a1)} \times \hat{v}_i) \cdot (\hat{v}_i \times \hat{v}_l)}{|\hat{v}_i \times \hat{v}_l|^2} \tan \varphi_l \\
 & + \frac{(\bar{r}^{(a1)} \times \hat{v}_l) \cdot (\hat{v}_i \times \hat{v}_l)}{|\hat{v}_i \times \hat{v}_l|^2} \tan \varphi_i + |\bar{C}_i^{(a1)}| + 2|\bar{C}_i^{(a1)}| \\
 & + |\bar{F}_{jR}^{(a1)}| + F^{[(a-1)1]} - |\bar{F}_{jR}^{[(a-1)1]}|, \quad F^{[(a-1)1]} > 0
 \end{aligned}$$

$$\begin{aligned}
 F^{(a1)} = & -|\bar{r}^{(a1)}| \cdot \hat{r} \cdot \hat{s} + \frac{(\bar{r}^{(a1)} \times \hat{v}_i) \cdot (\hat{v}_i \times \hat{v}_l)}{|\hat{v}_i \times \hat{v}_l|^2} \tan \varphi_l \\
 & + \frac{(\bar{r}^{(a1)} \times \hat{v}_l) \cdot (\hat{v}_i \times \hat{v}_l)}{|\hat{v}_i \times \hat{v}_l|^2} \tan \varphi_i + |\bar{C}_i^{(a1)}| + 2|\bar{C}_i^{(a1)}| \\
 & + |\bar{F}_{jR}^{(a1)}| - |\bar{F}_{jR}^{[(a-1)1]}|, \quad F^{[(a-1)1]} \leq 0
 \end{aligned} \quad (38)$$

In the end, consider transmission effect of net sliding force of Block  $ab$  ( $a \geq 2, b \geq 2$ ). The analysis method is the same as above. The calculation formula of Block  $ab$  is the combination of Eqs. (26) and (37) and has the similar form with Eqs. (26) and (38).

$$\begin{aligned}
 F^{(ab)} = & -|\bar{r}^{(ab)}| \cdot \hat{r} \cdot \hat{s} + \frac{(\bar{r}^{(ab)} \times \hat{v}_i) \cdot (\hat{v}_i \times \hat{v}_l)}{|\hat{v}_i \times \hat{v}_l|^2} \tan \varphi_l \\
 & + \frac{(\bar{r}^{(ab)} \times \hat{v}_l) \cdot (\hat{v}_i \times \hat{v}_l)}{|\hat{v}_i \times \hat{v}_l|^2} \tan \varphi_i + |\bar{C}_i^{(ab)}| + (|\bar{C}_i^{(ab)}| \\
 & - |\bar{C}_i^{[a(b-1)]}|) + |\bar{F}_{jR}^{(ab)}| + F^{[(a-1)b]} - |\bar{F}_{jR}^{[(a-1)b]}|, \\
 & F^{[(a-1)b]} > 0
 \end{aligned}$$

$$\begin{aligned}
 F^{(ab)} = & -|\bar{r}^{(ab)}| \cdot \hat{r} \cdot \hat{s} + \frac{(\bar{r}^{(ab)} \times \hat{v}_i) \cdot (\hat{v}_i \times \hat{v}_l)}{|\hat{v}_i \times \hat{v}_l|^2} \tan \varphi_l \\
 & + \frac{(\bar{r}^{(ab)} \times \hat{v}_l) \cdot (\hat{v}_i \times \hat{v}_l)}{|\hat{v}_i \times \hat{v}_l|^2} \tan \varphi_i + |\bar{C}_i^{(ab)}| + (|\bar{C}_i^{(ab)}| \\
 & - |\bar{C}_i^{[a(b-1)]}|) + |\bar{F}_{jR}^{(ab)}| - |\bar{F}_{jR}^{[(a-1)b]}|, \quad F^{[(a-1)b]} \leq 0
 \end{aligned} \quad (39)$$

To sum up, the net sliding force of each block in scattered-shape unstable rock mass sliding along both sides can be solved by iterative calculation. The introduction and sketch diagram of different model are illustrated in Fig. 9.

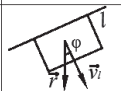

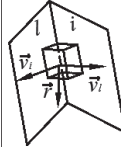
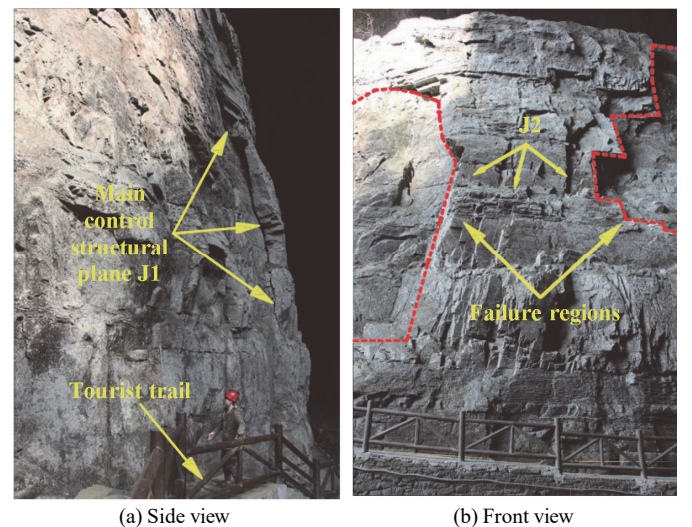
Block motion model	Sketch diagram	Judging condition	Introduction
Detachment form rock mass model		$\begin{cases} \hat{S} = \hat{r} \\ \hat{S} \cdot \hat{v}_i > 0 \end{cases}$	If $0^\circ < \varphi < 90^\circ$ , $\hat{S} \cdot \hat{v}_i > 0$ . There is no support from $l$ , block will detach from rock mass.
Along one-sided sliding model		$\begin{cases} \hat{S} = \hat{s}_i \\ \hat{r} \cdot \hat{v}_i \leq 0 \\ \hat{S} \cdot \hat{v}_i > 0 \end{cases}$	If $0^\circ < \varphi < 90^\circ$ , It will trigger shear strength (cohesion) and tensile strength of $j$ as resistance; If $90^\circ \leq \varphi < 180^\circ$ , It won't trigger shear strength but tensile strength of $i$ as resistance.
Along two-sided sliding model		$\begin{cases} \hat{S} = \hat{s}_{il} \\ \hat{S}_i \cdot \hat{v}_i \leq 0 \\ \hat{S}_l \cdot \hat{v}_i \leq 0 \\ \hat{S} \cdot \hat{v}_j > 0 \end{cases}$	In this case, block moves along the intersection line and must be in contact with $i$ and $l$ , while separated from $j$ . The specific resistance that generated by each structural plane needs to refer to the size of $\varphi$ and the judging rule is the same as above.

Fig. 9 Sketch diagram and introduction of different models

### 3. APPLICATION OF ENGINEERING EXAMPLE

#### 3.1 Basic Information of Unstable Rock Mass

This unstable rock mass (named W1) is located in Four-cave Gorge scenic area in Xianfeng County, Enshi Prefecture. Formation lithology is the inter-layer of middle-thick limestone and argillaceous siltstone of Lower Cambrian Tianheban Formation ( $\in 1t$ ), with the thickness of 0.4 ~ 0.6 m, colored by gray to dark gray. The occurrence of rock mass is  $95^\circ \angle 8^\circ$ , and two sets of joint (J1 and J2) are mainly developed. The joints are relatively rough, mainly filled with argillaceous and calcareous materials, with average cementation degree. The occurrence of J1 is  $203^\circ \angle 82^\circ$ , with 0.4 ~ 0.6 m spacing and extension length greater than 10 m. The occurrence of J2 is  $112^\circ \angle 85^\circ$ , with 0.3 ~ 0.5 m spacing and extension length of 5 ~ 7 m. The front view and side view of W1 is shown in Fig.10. This unstable rock mass is cut into relatively regular blocks by three groups of structural planes. The steeply inclined structural plane



(a) Side view

(b) Front view

Fig. 10 Panorama of W1 unstable rock mass

J1 at trailing edge is the main control structural plane. Some rock blocks on both sides and lower part have fallen off. Physical and mechanical parameters of rock mass obtained by laboratory tests are shown in Table 1.

**Table 1 Physical and mechanical parameters of rock mass**

$\gamma$ (kN/m <sup>3</sup> )	$c$ (kPa)	$\phi$ (°)	$f_i$ (kPa)
25.7	22.5	23	10

Note:  $\gamma$  is unit weight,  $c$  is cohesion,  $\phi$  is internal friction angle,  $f_i$  is tensile strength.

### 3.2 Stability Calculation of Scattered-shape Unstable Rock Mass

The basic procedures of stability analysis for scattered-shape unstable rock mass are: judge geometric mobility of blocks to judge motion mode of geometric movable blocks to analyze physical mobility of blocks to determine stability coefficients of blocks by SRM.

A reasonable geomorphological restoration of W1 unstable rock mass is carried out, as is illustrated in Fig. 11. From bottom to top, respective layer thickness is 1.2 m, 0.6 m, 0.6 m, 0.8 m, 0.6 m, and 1.2 m. The structural planes are arranged with equal width of 0.7 m, and the thickness of single block is 0.4 m.

#### 1. Judge geometric mobility of blocks

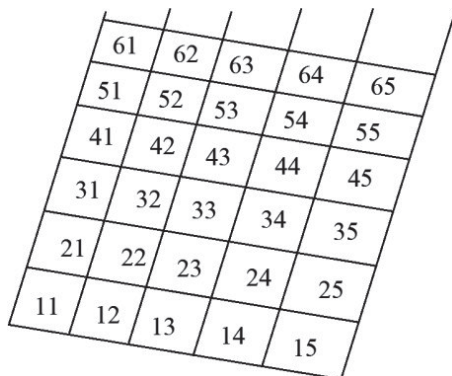
In traditional block theory, the necessary and sufficient condition for geometric movability of block is the block cone composed of structural planes only is infinite and the block cone composed of structural planes and free face is finite. Therefore, the infinite blocks should be determined at first. And then, the finite blocks among infinite blocks cut by free faces can be defined as geometric movable blocks.

- (1) Determine the unit normal vector  $\hat{n}_i$  of each structural plane  $P_i$  ( $P1203^\circ \angle 82^\circ$ ,  $P2112^\circ \angle 85^\circ$ ,  $P395^\circ \angle 8^\circ$ ).

$$\hat{n}_1 = (0.38693, -0.91155, 0.987688)$$

$$\hat{n}_2 = (0.923656, -0.37318, 0.087156)$$

$$\hat{n}_3 = (0.155839, -0.01363, 0.987688)$$



**Fig. 11 Calculation diagram of W1 unstable rock mass**

- (2) Solve direction vector  $\vec{I}_{ij}$  of intersecting line for structural planes.

$$\vec{I}_{12} = (-0.02751, 0.162271, 0.98635)$$

$$\vec{I}_{13} = (-0.89843, 0.403853, 0.14733)$$

$$\vec{I}_{23} = (0.3674, -0.8987, 0.045563)$$

- (3) Introduce directional parameter matrix  $[I]$ .

$$I = \begin{bmatrix} 0 & 0 & 1 \\ 0 & -1 & 0 \\ 1 & 0 & 0 \end{bmatrix}$$

- (4) Introduce discriminant matrix  $[T]$ .

Taking the digital coding “000” in block theory as an example, the corresponding discriminant matrix is:

$$T_{000} = \begin{bmatrix} 0 & 0 & 1 \\ 0 & -1 & 0 \\ 1 & 0 & 0 \end{bmatrix}$$

So far, the judging process whether the block cut by structural planes only is finite has been completed.

The judging process of finiteness for the block cut by free face is consistent with above. “A group of special ‘structural plane’ free face  $P$  is added and the occurrence is  $120^\circ \angle 85^\circ$ .”

Through the above steps, only a finite block numbered “0011” is searched out. Now, verify the mobility of this block.

The unit normal vector of  $P_4$  is:

$$\hat{n}_4 = (0.86273, -0.4981, 0.087156)$$

Except for the fore-mentioned  $\vec{I}_{ij}$ , other direction vectors of structural planes are:

$$\vec{I}_{14} = (-0.01012, 0.153792, 0.979147)$$

$$\vec{I}_{24} = (0.010887, -0.00531, -0.13812)$$

$$\vec{I}_{34} = (0.490777, 0.838526, 0.06586)$$

The  $[I]$  and  $[T]$  of Block “0011” are shown in Table 2 and 3, respectively.

**Table 2  $[I]$  of Block “0011”**

$I_{ij} \backslash P$	1	2	3	4
12	0	0	1	-1
13	0	-1	0	-1
14	0	1	1	0
23	1	0	0	1
24	-1	0	-1	0
34	-1	1	0	0

**Table 3**  $[T]$  of Block “0011”

$j \backslash P$	1	2	3	4
12	0	0	-1	-1
13	0	-1	0	-1
14	0	1	-1	0
23	1	0	0	1
24	-1	0	1	0
34	-1	1	0	0

It is clear that every row of the discriminant matrix has both “1” and “-1” in Table 3. which indicates that each edge is not the real edge of block. The block cone corresponds to an empty set. Hence, Block “0011” is finite. It satisfies the infinity cut by structural planes only and the finity cut by structural plans and free face meanwhile. In conclusion, Block “0011” is the only geometric movable block of W1.

2. Judge motion mode of geometric movable block

Assuming W1 is affected by gravity in natural state,  $\hat{r} = (0, 0, -1)$ ,  $\vec{r} = (0, 0, -\gamma v)$ .  $\gamma$  is the volumetric weight and  $v$  is the volume. The respective unit normal vector pointing to block itself of each structural plane is:

$$\hat{v}_1 = (-0.38693, -0.91155, 0.987688)$$

$$\hat{v}_2 = (0.923656, -0.37318, 0.087156)$$

$$\hat{v}_3 = (-0.155839, 0.01363, -0.987688)$$

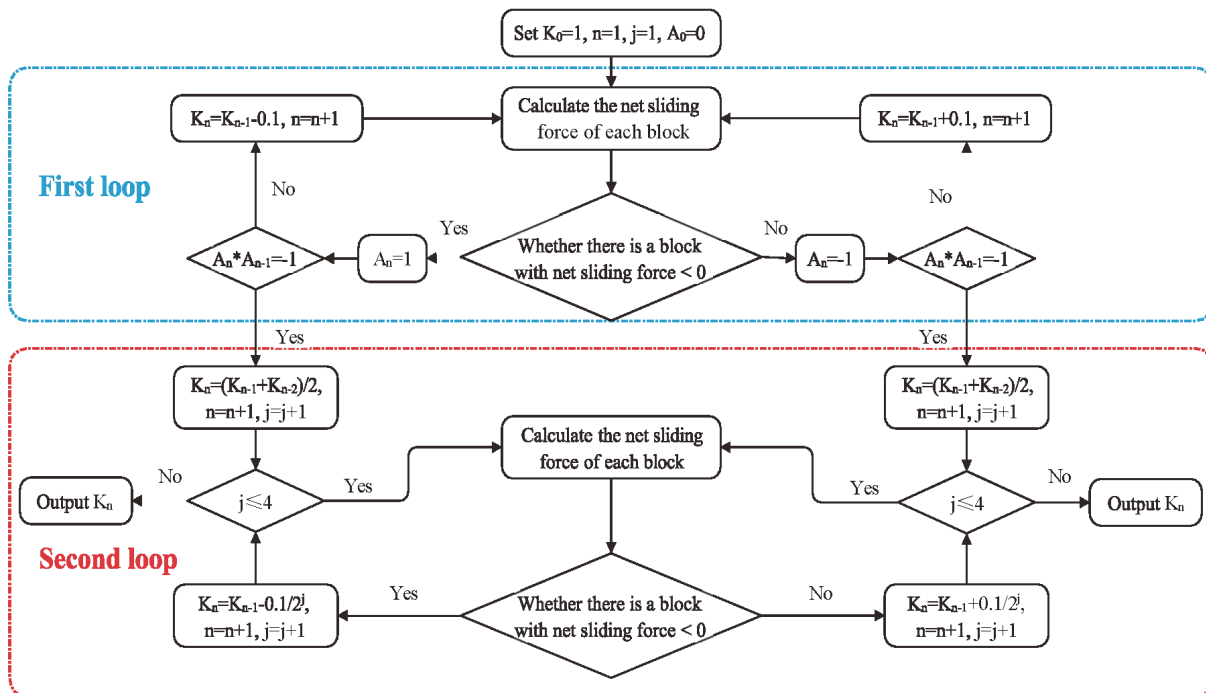
Obviously, when  $\hat{s} = \hat{r}$ ,  $\hat{s} \cdot \hat{v}_1 < 0$  and  $\hat{s} \cdot \hat{v}_2 < 0$  which does not match Eq. (9), the mode of detachment from rock mass will not appear. It is easy to learn that  $\hat{r} \cdot \hat{v}_3 > 0$ . If Block “0011” slides along  $P_1$  only, i.e.,  $\hat{s} \cdot \hat{v}_1 < 0$ , which does not match Eq. (13). If Block “0011” slide along  $P_2$  only, i.e.,  $\hat{s}_2 \cdot \hat{v}_2 < 0$ ,

which does not match with Eq. (13), either. Therefore, the motion mode of Block “0011” is along double-sided sliding. Since bedding plane is nearly horizontal, it can be judged that the block slides along  $P_1$  and  $P_2$  without resorting to Eq. (28).

3. Determine stability coefficients of blocks by SRM

The basic idea of SRM is to divide the strength parameters by a certain reduction factor, and the reduced strength parameters are used in analysis, which is repeated iteratively. When the model does not converge at a certain reduction factor, which can be defined as the stability coefficient (Cundall and Strack 1979). The process of using SRM to solve the stability of scattered-shape unstable rock mass is shown in Fig. 12. Two loops are used in this process. The first loop is to determine the range of stability coefficients, and the second loop is to gradually approach the true stability coefficient by dichotomy. Set the increment step of reduction factor to 0.1. Exit the calculation procedure when 4 dichotomous reductions occur (i.e.,  $j > 4$ ), and the accuracy of stability coefficient is  $2^{-4} = 0.0625$ . In the calculation procedure, it is necessary to input the data such as unit normal vector of each structural surface pointing to inside of block, the physical and mechanical parameters of rock mass, and the area of each contact surface of block. Based on the judgement of block motion mode, the calculation is carried out according to the net sliding force equations corresponding to different motion modes, as shown in Sections 2.2, 2.3, and 2.4. The stability coefficient of W1 is automatically iteratively calculated by Visual Basic programming language combined with SRM. The calculation results of reduced stability coefficient in every step and net sliding force of each block are shown in Fig. 13.

In Fig. 12,  $K_0 = 1$  is the initial reduction factor, that is, the unreduced situation.  $K_n$  is reduction factor after calculation, n is the cycle number and the initial value is 1.  $A_n$  is judgement factor and j is the number of dichotomies.



**Fig. 12** Flowchart of stability coefficient calculation by SRM



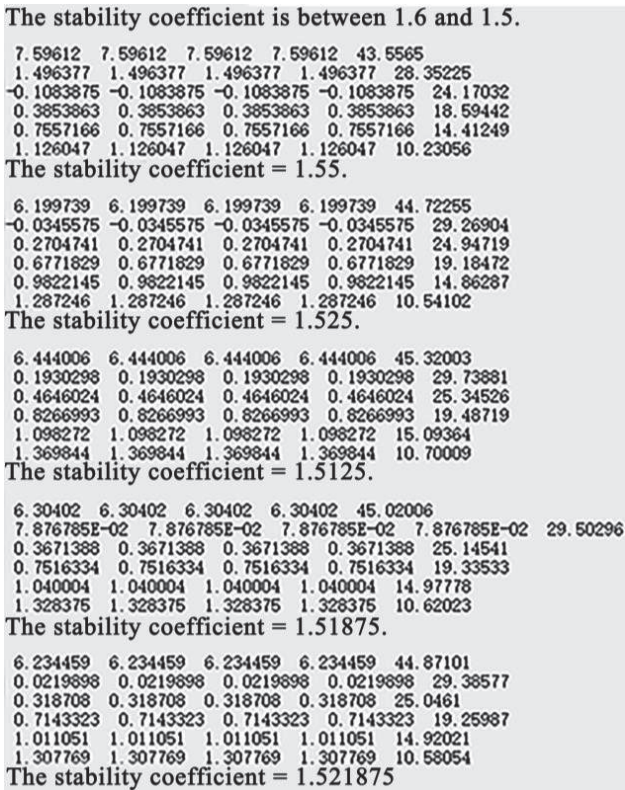


Fig. 13 Calculation results of stability coefficient and net sliding force

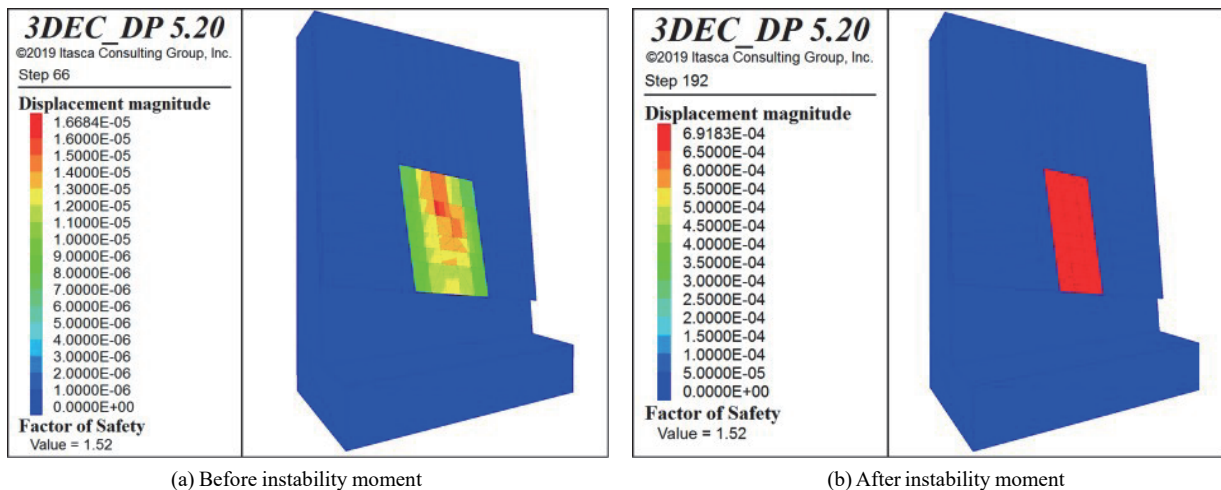
As is described in Fig. 13, at different iterative calculation steps, stability coefficient on each row and column coordinates corresponds to the block at the same position in Fig. 10. After multiple iterative calculations, the stability coefficient of W1 is determined as 1.521875. The net sliding force of blocks in the rightmost column increases from bottom to top, so the failure process is in the form of spalling layer by layer when mechanical parameters of structural planes are gradually weakened. When the reduction factor is 1.55, in the region from the third row and the fourth column on the left, net sliding force of block begins to decrease to negative, indicating that the blocks have been unstable. When the net sliding force of bottom block is greater

than 0, it can be transmitted to upper block. If the net sliding force of upper block is still less than 0, it isn't enough to resist sliding, although the net sliding force of bottom block is more than 0. It can be considered that blocks in this part have undergone holistic failure. As a result, when the reduction factor is 1.521875, Blocks 44 and below blocks in Fig. 11 can be considered as unstable already, which is consistent with the failure area in Fig. 10(b), where two-row blocks on right side haven't yet been destabilized. Theoretical calculation result shows only one-row blocks haven't been destabilized. Structural planes are set at equal intervals in the theoretical model, but they are irregular and with non-uniform spacing in reality, which leads to errors in the calculation result.

### 3.3 Numerical Simulation for Verification Analysis

The stability, deformation and failure process of W1 in natural state were simulated and analyzed through 3DEC. The model is 15 m high, 10 m long and 6 m wide. Rigid body model of rock blocks and elastoplastic Mohr-Coulomb (M-C criterion) failure were used in numerical simulation. The size and distribution of structural planes are the same with Fig. 11. The parameters of model are shown in Table 1. The boundary condition is bound the displacements in all directions of blocks except the unstable rock mass. Displacement magnitude diagram and joint shear force magnitude diagram of model before and after the instability moment are shown in Figs. 14 and 15, respectively.

The overall stability coefficient obtained of W1 by numerical simulation is 1.52, which is very close to the previous calculation result (1.521875) of theoretical model. It suggests that the theoretical model and numerical simulation have a high degree of consistency under the same calculation conditions, and the reliability of theoretical model has been well verified. Maximum displacement of model is only  $1.66 \times 10^{-5}$  m before failure and  $6.9 \times 10^{-4}$  m after failure, which is located in the middle region. Maximum shear force mainly gathers at middle region of rock mass before instability moment while disappears after that. The maximum shear force appears at the bottom of left boundary, which is also the first signal of local block to break. Subsequently, rock mass will be broken in the form of spalling layer by layer from bottom to top.



(a) Before instability moment

(b) After instability moment

Fig. 14 Displacement magnitude diagram of model before and after the instability moment

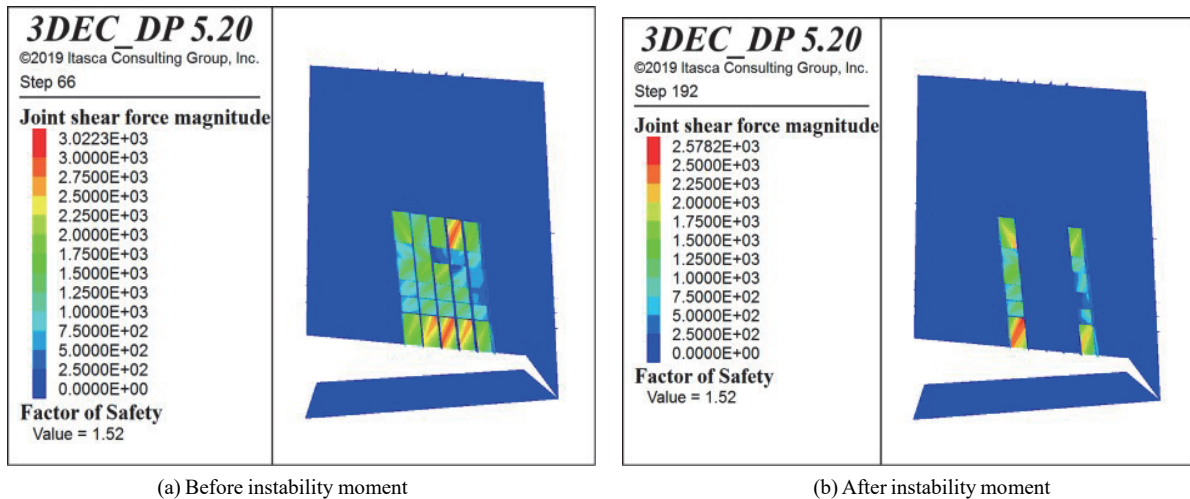


Fig. 15 Joint shear force magnitude diagram of structural planes before and after the instability moment

### 3.4 Discussion

Compared with traditional block theory, the improved block theory takes into account the cohesion and tensile strength of the structural plane. However, both of them have a limitation, that is, only the translational slip failure mode of the rock blocks along structural planes is considered. There is a lack of consideration for another failure mode of block-rotational failure, which is often referred to as tipping failure. At present, the rotational failure of rock blocks has been studied based on traditional block theory, while little research considers the cohesion and tensile strength of structural planes. If the block theory could both consider rotational failure mode and the cohesion and tensile strength of structural planes in future, it would be enriched and more applicable in practical engineering.

## 4. CONCLUSIONS

The unstable rock mass cut by gently-dipping structural planes and controlled by steep-dipping structural planes is defined as scattered-shape unstable rock mass. Rock blocks are always scattered and arranged in small size. The deformation and failure mechanical model under natural condition of scattered-shape unstable rock mass has been constructed by improved block theory, which takes into account the cohesion and tensile strength of structural planes. Based on unbalanced thrust method and vector analysis method, the calculation formula of net sliding force for blocks with three motion modes were deduced.

The stability coefficient of engineering example (W1) was determined as 1.521875 according to theoretical model. That is almost identical with the result (1.52) obtained by numerical simulation. The failure mode of W1 has been confirmed as spalling layer by layer at the same time. The instability regions got by theoretical simulation and numerical simulation are in coincident with reality. By means of instance analysis, the proposed method for stability analysis for scattered-shape rock mass is feasible.

## ACKNOWLEDGEMENTS

All the authors acknowledge the support by National Natural Science Foundation of China (Grant Nos. 41672313 and 41972289).

## FUNDING

The National Natural Science Foundation of China (Grant Nos. 41672313 and 41972289).

## DATA AVAILABILITY

The data and/or computer codes used/generated in this study are available from the corresponding author on reasonable request.

## CONFLICT OF INTEREST STATEMENT

The authors state that there are no financial interests or personal relationships that might influence the work reported in this paper.

## REFERENCES

- Cai, J., Yan, E., Wang, Z., Yang, J., and Tang, R. (2014). "Study of cantilever beam limit equilibrium model of anti-dip layered rock slopes." *Rock and Soil Mechanics*, **35**(Supp.1), 15-28. <https://doi.org/10.16285/j.rsm.2014.s1.003>
- Chen, H., Wang, R., and Tang, H. (2003). "Review on current situation to study and trend of dangerous rock mass." *Journal of Chongqing Jiaotong University*, **22**(3), 18-22.
- Chen, H., Tang, L., Zhang, R., Tang, H., and Wu, R. (2013). "Mutation instability model of perilous rock and calculation methods for corresponding dynamic parameter." *Applied Mechanics and Materials*, **249/250**, 1030-1039. <https://doi.org/10.4028/www.scientific.net/amm.249-250.1030>
- Cundall, P.A. and Strack, O.D.L. (1979). "A discrete numerical model for granular assemblies." *Geotechnique*, **29**(1), 47-65. <https://doi.org/10.1680/geot.1979.29.1.47>
- Dai, Z., Liu, Z., Liu, C., and He, M. (2008). "Numerical analysis of soil slope stability considering tension and shear failures." *Chinese Journal of Rock Mechanics and Engineering*, **27**(2), 375-382.
- Du, Y., Yan, E., Cai, J., and Hu, X. (2019). "Reliability analysis method on unstable rock mass controlled by discontinuous

- structure.” *Journal of Harbin Institute of Technology*, **51**(8), 120-127.  
<https://doi.org/10.11918/j.issn.0367-6234.201805025>
- Goodman, R.E. and Shi, G.H. (1985). *Block Theory and Its Application to Rock Engineering*, Prentice Hall, Upper Saddle River.
- Hu, M., Yan, E., Yang, J., and Li, Y. (2011). “Stability assessment of unstable rock blocks at Nanmenwan in Wuxi country.” *Journal of Engineering Geology*, **19**(3), 397-403.
- Huang, B., Zhang, Z., Yin Y., and Fei, M. (2016). “A case study of pillar-shaped rock mass failure in the Three Gorges Reservoir Area, China.” *Quarterly Journal of Engineering Geology and Hydrogeology*, **49**(3), 195-202.  
<https://doi.org/10.1144/qjegh2015-034>
- Huang, R. (2009). “Mechanism and geomechanical modes of landslide hazards triggered by Wenchuan 8.0 earthquake.” *Chinese Journal of Rock Mechanics and Engineering*, **28**(6), 1239-1249.
- Huang, R., Liu, W., Gong, M., and Zhou, J. (2010). “Study on trees resistance effect test on rolling rock blocks.” *Chinese Journal of Rock Mechanics and Engineering*, **29**(S1), 882-891.
- Hungr, O., Leroueil, S., and Picarelli, L. (2014). “The Varnes classification of landslide types, an update.” *Landslides*, **11**, 167-194.  
<https://link.springer.com/article/10.1007/s10346-013-0436-y>
- Lai, J. and Fang, Y. (2011). “Stability analysis of rock slope with extroversion joint considering tensile strength.” *Journal of Logistical Engineering University*, **27**(6), 7-12.  
<https://doi.org/10.3969/j.issn.1672-7843.2011.06.002>
- Lin, P., Liu, X., Hu, Y., Xu, W., and Li, Q. (2013). “Deformation stability analysis of Xiluodu arch dam under stress-seepage coupling condition.” *Chinese Journal of Rock Mechanics and Engineering*, **32**(6), 1145-1156 (in Chinese).
- Liu, C., Liu, X., Peng, X., Wang, E., and Wang, S. (2019). “Application of 3D-DDA integrated with unmanned aerial vehicle — laser scanner (UAV-LS) photogrammetry for stability analysis of a blocky rock mass slope.” *Landslides*, **16**(9), 1645-1661.  
<https://doi.org/10.1007/s10346-019-01196-6>
- Liu, C. and Zhang, M. (1999). “Research on the control engineering of Lianziya dangerous rockbody in the Three Georges of Yangtze River.” *Chinese Journal of Rock Mechanics and Engineering*, **18**(5), 497-502.
- Liu, X., Han, G., Wang, E., Wang, S., and Kumar, N. (2018). “Multiscale hierarchical analysis of rock mass and prediction of its mechanical and hydraulic properties.” *Journal of Rock Mechanics and Geotechnical Engineering*, **10**(4), 694-702.
- Moon, T., Oh, J., and Mun, B. (2014). “Practical design of rockfall catchfence at urban area form a numerical analysis approach.” *Engineering Geology*, **172**, 41-56.  
<https://doi.org/10.1016/j.enggeo.2014.01.004>
- Shi, G.H. and Goodman, R.E. (1989). “Generation of two-dimensional discontinuous deformation analysis for forward modelling.” *International Journal for Numerical and Analytical Methods in Geomechanics*, **13**(4), 359-380.  
<https://doi.org/10.1002/nag.1610130403>
- Wang, Z., Yan, E., Yin, X., Zhang, X., and Tang R. (2014). “Study on collapse mechanism of anti-inclined rock slope: A case study of Honglianchi Iron Mine slope in Hefeng, Hubei province.” *Journal of Central South University, Science and Technology*, **45**(7), 2295-2301.
- Wang, J., Shi, Y., Wang, W., Cheng, Y., and Li, C. (2014). “Basic features and prevention measures of a giant unstable rock mass at Jiexu hydropower station, Yarlung Zangbo River.” *Chinese Journal of Rock Mechanics and Engineering*, **33**(S1), 2635-2640.
- Zhang, L. and Jia, C. (2019). “Application of key block theory based on force transfer algorithm in underground cavern rock support.” *Journal of Anhui Jianzhu University*, **27**(4), 1-7. <https://doi.org/10.11921/j.issn.2095-8382.20190401>

